

Interstellar Dust at the Magnetic Wall of the Heliosphere. II.

Priscilla C. Frisch

Department of Astronomy and Astrophysics, University of Chicago, Chicago, IL 60637.

frisch@oddjob.uchicago.edu

ABSTRACT

October 8, 2018

Two sets of data show that small interstellar grains captured in interstellar magnetic fields, \vec{B}_{IS} , draped over the heliosphere appear to polarize the light of nearby stars. The polarizing grains couple to \vec{B}_{IS} , while larger grains couple to the cloud velocity. The maximum polarization direction, P_{max} , is offset in ecliptic longitude by $\Delta\lambda \sim +35^\circ$ from the upwind direction, and the polarization peak is enhanced for stars near the ecliptic plane. A band of weak polarization stretches through the southern ecliptic hemisphere between the P_{max} region and the downwind direction. The P_{max} direction indicates that \vec{B}_{IS} at the heliosphere is directed towards $\ell \sim 105^\circ$, forming an angle of $\sim 75^\circ$ with the inflowing gas. Grain alignment appears stable as the grains approach the heliosphere. The disruption of grain alignment in the tenuous local interstellar material (ISM) by stochastic collisions is ~ 600 times slower than in the denser clouds for which grain alignment theory has been developed, however grain alignment mechanisms are still fast, and are boosted by compression of \vec{B}_{IS} at the heliosphere. The polarization vanishes where the outer heliosheath magnetic fields become tangled or reconnect. A similar offset seen in energetic neutral atoms may form inside of the polarization region, where the plasma is pinched by opposing magnetic fields. The composition of dust in the interstellar cloud surrounding the solar system appears to be similar to olivines, and significant quantities of carbonaceous grains can be ruled out.

1. Introduction

The symmetry of the interaction between the heliosphere and interstellar material is determined by three fundamental phenomena: the solar wind (which loosely traces eclip-

tic coordinates and is variable), the inflow direction of interstellar gas, and the interstellar magnetic field. This note is focused on the polarization of interstellar dust grains at the heliosphere, which appear to mark the third, and most poorly known, of these three parameters.

The heliosphere is the “bubble” occupied by the solar wind (e.g. Zank 1999). The heliosphere nose location is provided by the upwind direction of the flow of neutral interstellar gas through the solar system. Ulysses He^o data provide the best value for this velocity, which in the solar rest frame corresponds to -26.3 km s^{-1} from the upwind direction $\lambda=254.7\pm 0.5^\circ$, $\beta=5.2\pm 0.2^\circ$ (ecliptic coordinates; in galactic coordinates the upwind direction is $\ell=3.3^\circ$, $b=15.9^\circ$, Witte 2004; Möbius et al. 2004). Interstellar dust grains have been observed flowing through the solar system by Ulysses (at all ecliptic latitudes), Galileo, and Cassini (Grun et al. 1993; Baguhl et al. 1996; Grün et al. 2005; Frisch et al. 1999, F99). The inflowing larger grains are at the gas velocity, and have an upwind direction of $\lambda=259^\circ$, $\beta=8^\circ$ ($l=8.3^\circ$, $b=12.9^\circ$). The Ulysses and Galileo data were acquired in the 1990’s, during a time when the solar magnetic polarity ‘defocused’ smaller charged grains (radius $a \lesssim 0.2 \mu\text{m}$, Landgraf 2000). The termination shock (TS) of the solar wind, where the solar wind becomes subsonic, was recently crossed by Voyager 1 at $\sim 94 \text{ AU}$ (e.g., Stone et al. 2005; Burlaga et al. 2005; Decker et al. 2005). Beyond that $\sim 50 \text{ AU}$, the heliopause separates solar wind and interstellar plasmas; outside of the heliopause, interstellar field lines drape over the heliosphere, following compression in the outer heliosheath regions by factors of 2–5 (Linde 1998; Pogorelov et al. 2004).

The primary data on the interstellar magnetic field near the Sun, \vec{B}_{IS} , have been observations of weakly polarized, $P \sim 0.02\%$, light from stars within $\sim 30 \text{ pc}$ and in the interval $l \sim 330^\circ \pm 60^\circ$, $b \sim 0^\circ \pm 50^\circ$ (Tinbergen 1982, T82, also see Frisch 1990). The polarization is produced by magnetically aligned small charged interstellar dust grains, producing a birefringent medium where the opacity parallel to \vec{B}_{IS} is lower than the opacity perpendicular to \vec{B}_{IS} , resulting in a polarization maximum when the sightline is perpendicular to the magnetic field direction, \hat{k}_{B} (§4). The location of the polarization patch coincides with most of the mass of nearby interstellar material (ISM, Frisch & York 1983), and with the upwind direction of the bulk flow of ISM past the solar location (Frisch et al. 2002).

I recently discovered that this weak polarization coincides with the heliosphere nose region, and suggested an origin associated with magnetically aligned small grains trapped in the interstellar field lines at the magnetic wall of the heliosphere (Frisch 2005, Paper I). Paper I showed that the region of maximum polarization is offset by $\delta\lambda \sim +35^\circ$ along the ecliptic plane from the large-grain inflow direction. *Evidently, at the heliosphere small grains with large charge-to-mass ratios, Q/M , trace the interstellar magnetic field direction, \vec{B}_{IS} ,*

while large grains with low Q/M trace the interstellar cloud velocity.

The present note provides support for this hypothesis that the polarization originates with interstellar dust at the heliosphere, using additional polarization data (§3), evidence for olivine grains with stable alignment as the grains approach the heliosphere (§§2.3, 4.1), and a discussion of the still-uncertain grain alignment mechanisms in the context of the heliosphere interaction with the ISM (§4).

Charged ISDGs spin rapidly and will always be aligned so that the observed polarization, P , of starlight is parallel to the magnetic field direction, \hat{k}_B , regardless of the alignment mechanism (e.g., Lazarian 2003, §4). Evidently aligned grains do not behave like dumb compass needles, but rather trace the coupling between the grain angular momentum and \vec{B}_{IS} . Thus, the T82 data indicate that \hat{k}_B is approximately parallel to the galactic plane and oriented towards $\ell \sim 90^\circ$ (see Fig. 6 of T82), or as found here $\ell \sim 105^\circ$. A similar orientation for \hat{k}_B is indicated by the 2.6 kHz Langmuir emission events observed by Voyager (Kurth & Gurnett 2003, KG03). Triangulation by Voyager 1 and 2 show that the dozen emission events detected in the 1990’s arise in the outer heliosphere at ~ 100 AU from the Sun, and that these dozen emission events are approximately aligned with the galactic plane (see, e.g., Cairns 2004, for a discussion of formation mechanisms).

2. Interstellar Gas, Magnetic Field, and Dust at Solar Location

2.1. Gas

The tenuous nature of the interstellar cloud surrounding the Sun reduces the collisional disruption of grain alignment (§4.1). The density and ionization of the ISM at the solar location are found from radiative transfer (RT) models that are constrained by observations of ISM both inside and outside of the heliosphere (Slavin & Frisch 2002; Frisch & Slavin 2003; Frisch & Slavin 2005; Slavin & Frisch 2006b,a, SF02,FS03,FS05,SF06).¹ While a range of tested equilibrium models reproduce the general properties of tenuous clouds, the models which provide the best fits to the local interstellar cloud (LIC) data, have $n(\text{H}^\circ) \sim 0.2 \text{ cm}^{-3}$, $n(\text{e}) \sim 0.1 \text{ cm}^{-3}$, $n(\text{He}^\circ) \sim 0.015 \text{ cm}^{-3}$, and fractional ionizations $\chi(\text{H}) \sim 0.29$, $\chi(\text{He}) \sim 0.47$.² However somewhat lower ionizations, $n(\text{e}) \sim 0.07 \text{ cm}^{-3}$, can not yet be ruled out conclusively (FS05). The Ulysses He° data give a LIC temperature at the heliosphere of $6300 \pm 340 \text{ K}$

¹The SF02 radiative transfer models are based on Version 90.05 of the CLOUDY code.

²The fractional ionization of H is given by $\chi(\text{H}) = \text{H}^\circ / (\text{H}^\circ + \text{H}^+)$, etc.

(Witte 2004). If observed from a distance, the warm partially ionized local ISM within ~ 35 pc, $N(\text{H}) \lesssim 10^{19} \text{ cm}^{-2}$, may appear as either warm ionized or warm neutral material (WIM, WNM).

Interstellar dust grain abundances in generic warm ISM are relatively invariant the ionization level of the gas, and approximately 25%–30% of the infrared emission from dust within ~ 150 pc is formed in warm H^+ gas. This is shown by observations of WNM and WIM in a high-latitude region with sparse ISM, where comparisons are made between 100–1000 μm DIRBE and FIRAS infrared emission, H° 21-cm emission (Leiden data), and H^+ $\text{H}\alpha$ emission (WHAM data, Lagache et al. 2000). Column densities for LIC-like clouds, $N(\text{H}) < 10^{18} \text{ cm}^{-2}$, are not usually resolved in H° 21-cm or $\text{H}\alpha$ measurements.

The LIC velocity, $V_{\text{LSR}} \sim 15\text{--}20 \text{ km s}^{-1}$ in the Local Standard of Rest (LSR, Frisch et al. 2002), is a factor in dust composition, since high cloud velocities are associated with enhanced gas-phase abundances of refractory elements and grain destruction in interstellar shocks (Routly & Spitzer 1952; Jones et al. 1996). For comparison, over 25% of the H° mass detected in the Arecibo Millenium survey (Heiles & Troland 2003) is at $V_{\text{LSR}} > 10 \text{ km s}^{-1}$. Local interstellar gas, therefore, appears to be typical dust-containing tenuous intermediate velocity partially ionized ISM.

2.2. Magnetic Field

Linde (1998) has modeled the distance of the termination shock (TS) in the direction of the Voyager 1 motion, and found that $|\vec{B}_{\text{IS}}| \sim 1.5 \mu\text{G}$ yields a TS distance of 94 AU, which agrees with the recently measured Voyager 1 value (§1). I argued that \vec{B}_{IS} at the Sun should be similar to the uniform component of B_{IS} inferred from pulsar data, $|\vec{B}_{\text{IS}}| \sim 1.6 \mu\text{G}$, which dominates low density interarm regions such as surrounding the Sun (Frisch 1990). However stronger fields are indicated, $|\vec{B}_{\text{IS}}| \sim 2.6 \mu\text{G}$, if equipartition between thermal and magnetic pressure applies. The value $|\vec{B}_{\text{IS}}| = 1.5 \mu\text{G}$ will be used in the following discussions.

2.3. Dust Composition

The interaction between ISDGs and the heliosphere depends on the dust charge, mass, and composition. In this section the results of radiative transfer models of the local ISM are compared with a reference abundance for the ISM, here assume to be solar abundances, to determine the dust composition. The following section gives the gas-to-dust mass ratio

calculated from the same assumptions. Unfortunately, both solar abundances and the ISM composition, generally assumed to be the summed abundances of the gas and dust, are highly uncertain. For instance, estimates of the solar ratio for O/H vary by $\sim 30\%$ (Grevesse & Sauval 1998; Holweger 2001; Lodders 2003; Asplund et al. 2005). Also, gas and grains may decouple in transient violent interstellar phenomena (e.g. Slavin et al. 2004).

The predicted LIC gas-phase abundances of C, N, O, Mg, Al, Si, and Fe are listed in Table 1 for the best-fitting RT models 2 and 8 (SF02). Comparisons between the gaseous Fe, Mg, Si, and O abundances and solar abundances then yield underabundances of Fe, Mg, Si, and O in the gas within ~ 1 pc of the Sun towards ϵ CMa. For this discussion, the abundances presented in Lodders (2003, L03) are utilized. The short length of the local ISM towards ϵ CMa (~ 1 pc) contains two velocity components separated by ~ 8 km s $^{-1}$ (Gry & Jenkins 2001),³ but is characteristic of tenuous ISM.

The atoms “missing” from the gas, and therefore inferred to be in the dust, show approximately equal amounts of Fe, Mg, and Si, or Fe:Mg:Si $\sim 1:1:1$ (column 4 of Table 1). The best LIC dust constraints are the Mg:Si:Fe ratios, because the RT models correct for H $^+$. These ratios Fe:Mg:Si $\sim 1:1:1$ suggest an olivine-type mineral, possibly amorphous olivine similar to $\sim 85\%$ of the dust mass towards SgrA* (see below).

Similar results are reached if the Asplund et al. (2005) solar abundances are used, except that there is a surplus of C in the gas phase (see SF06), the O:Si ratios are reduced in the dust, and the gas-to-dust mass ratio $R_{g/d}$ becomes excessively large (§2.4).

An improved understanding of the reference abundance for local ISM will permit stricter constraints on the LIC dust based on the ratio O:Si. The inferred O abundances from the models 2 and 8 indicate somewhat higher O abundances in the dust than required by olivines, since O:Mg, O:Si, and O:Fe are ~ 5 – 6 , rather than the value ~ 4 expected for olivines. Evidently for olivine grains and L03 abundances, where O/H=575 PPM, between one and two O atoms are “missing” from both the dust and gas. A value O/H=520 would be required to eliminate these missing O atoms.

The LIC grains are not carbonaceous. The RT models 2 and 8 give C abundances that are approximately solar, suggesting that graphite is absent from LIC dust, perhaps because it did not survive the LIC acceleration mechanism (Table 1, also see Slavin & Frisch 2006b). The absence of local graphite does not affect the polarization discussion, since graphite does not contribute to polarization in the global ISM (Whittet 2004).

Silicates are a widespread constituent of interstellar dust. A silicate mixture consisting of

³Radiative transfer models of the LIC, alone, are now under development (SF06b).

84.9% amorphous olivine (MgFeSiO_4) and 15% amorphous pyroxene ($\text{MgFeSi}_2\text{O}_6$), by mass, fits observations of a $9.7 \mu\text{m}$ infrared feature in Sgr A* (Kemper et al. 2004). The amorphous olivine grains forming 85% of the grain mass towards SgrA* must be robust, or they would not dominate, which lends credibility to the possibility that local ISDGs are amorphous olivines that have survived the process that accelerated the moderate velocity ISM surrounding the Sun. Silicates are also found in evolved stars such as Mira variables (e.g. Dorschner & Henning 1995; Chiar & Tielens 2006). Additional evidence of widespread silicates are provided by models of the grain populations, in terms of size and composition, required to fit extinction measurements, diffuse infrared emission, and abundance constraints for the diffuse ISM (Zubko et al. 2004, ZDA). The ZDA COMP-GR-FG model, consisting of silicates (MgFeSiO_4), graphite, and a small amount PAHs, provides a good fit to the extinction and IR emission data if ISM abundances are comparable to F and G star abundances. The silicates in the ZDA COMP-GR-FG model have $a < 0.25 \mu\text{m}$, with most of the grain mass contained in grains with $a \sim 0.06 - 0.25 \mu\text{m}$, however a significant fraction of silicate grains with $a \lesssim 0.01 \mu\text{m}$ are present. The small amount of PAHs required by the COMP-GR-FG are allowed by the LIC C data, depending on the assumed solar C abundance.

2.4. Gas-to-Dust Mass Ratio, $R_{g/d}$

The above arguments used to derive grain composition assume that dust and gas have been fully mixed over the cloud lifetime. A check on this assumption is the gas-to-dust mass ratio, $R_{g/d}$, in local ISM, which can be examined in several ways. (1) The first method compares spacecraft *in situ* measurements of the ISDG mass with the gas mass determined from RT models. Updating the F99 discussion with more recent spacecraft results (Landgraf et al. 2000; Altobelli et al. 2004) yields $R_{g/d} < 130$, where the upper limit holds because small charged ISDGs are excluded from the solar system. (2) $R_{g/d}$ can also be determined from comparisons between the RT models and solar abundances. For the L03 solar abundances, model 8 yields $R_{g/d} = 186$. If instead the ISM reference O abundance is $\text{O}/\text{H} = 520$ (see above), model 8 gives $R_{g/d} = 210$. For either case the *in situ* measurements and model 8 predictions disagree. For comparison, the Asplund et al. abundances yield $R_{g/d} = 330$, due to the lower solar abundances for Mg, Si, and Fe of $\sim 20\%$, compared to L03. The difference between (1) and (2) estimates of $R_{g/d}$ may indicate a grain population is present that has not been coupled to the gas over the cloud lifetime, such as expected if the LIC has been shocked to high LSR velocities (Frisch 1981, F99). Evidently the tiny grains are disproportionately destroyed by sputtering so that $R_{g/d}$ derived from *in situ* data may not be significantly overestimated.

A third basis for understanding $R_{g/d}$ in the LIC uses the silicate component of the ZDA COMP-GR-FG model as a model for LIC dust. The silicate component in the COMP-GR-FG model alone yields $R_{g/d}=251$, while the silicate and PAHs together give $R_{g/d}=233$. The other constituents in the COMP-GR-FG model, graphite, water ice, and organics, are not required by “missing” atoms of RT models 2 and 8. If allowance is made for differences between the F and G star abundances of ZDA and the L03 abundances assumed here, and the F and G star abundances are compared to model 8, then the $R_{g/d}=229$ for model 8 is similar to the COMP-GR-FG predictions for the silicate and PAHs combined.

The above arguments indicate that the local ISM gas phase abundances given by RT models 2 and 8 of SF02 are consistent with the ZDA COMP-GR-FG silicate grains, providing that graphite is absent from the LIC. The silicate grains in the ZDA COMP-GR-FG model have $a < 0.4 \mu\text{m}$, compared to *in situ* LIC data showing grains up to $a \gtrsim 1.1 \mu\text{m}$ (F99). Disproportionate percentages of large grains are predicted by the Slavin et al. (2004) grain destruction models for regions inside of supernova remnants, where the large grains survived multiple shocks associated with such environments. This scenario agrees with models of the LIC as a fragment of a superbubble shell, forming ~ 4 million years ago out of debris left over from a prior generation of star formation in the Scorpius-Centaurus Association (Frisch 1981, 1995, 1996).⁴

3. Characteristics of the Polarization

The analysis of Paper I has been repeated with the inclusion of polarization data from Piirola (1977), as well as the (Tinbergen 1982) data. (Paper I was based only on the Tinbergen data.) These combined data sets yielded a sample of 202 nearby stars; 86% of the stars are within 40 pc. Note that these distances are based on Hipparcos data, which may differ from distances in the original pre-Hipparcos publications. The two data sets have 45 stars in common. Both data sets were acquired during the solar minimum conditions of 1973–1974,⁵ when the solar magnetic polarity was north pole positive (i.e. $A > 0$, field lines emerging at the north pole, Frisch et al. 2005). The typical 1σ measurement uncertainties for these data are $\sim 6 - 17 \times 10^{-5}$ degree of polarization (Channels I and II), but only values with

⁴Please note that Breitschwerdt et al. (2000) were incorrect when they stated “...an alternative scenario by Frisch (1995, 1996), ... has pictured the Local Bubble to be an appendix of the Loop I superbubble which expanded into a low density interarm region, an idea that had been proposed earlier by Bochkarev (1987).”. I proposed this idea in 1981, and Bochkarev referenced my earlier paper.

⁵The Piirola data were acquired in 1974 (Piirola 1977), while the Tinbergen data were acquired during 1973 (J. Tinbergen, private communication).

uncertainties $\lesssim 7 \times 10^{-5}$ are used here. The linear Stokes parameters U and Q provided in the original papers give P and the polarization position angle, $\theta_C = 0.5 \arctan(U/Q)$, which is the angle of the observed electric vector as measured positive in a counter-clockwise direction from the north celestial pole. The position angle, θ_C , indicates a value in the celestial coordinate system.

The primary results of Paper I are shown in Fig. 1, but now including both Tinbergen (1982) and Piirola (1977) data. The three panels show the ecliptic longitude, λ , dependence of polarization P (top), position angle θ_C (middle, θ_C in celestial coordinates), and the P - β correlation coefficient ($C_{P\beta}$, bottom, β is ecliptic latitude). The filled dots represent values averaged over stars within $\pm 50^\circ$ of the ecliptic plane ($|\beta| < 50^\circ$), and within $\pm 20^\circ$ of the central ecliptic longitude, λ_0 . An artificial smoothing of the points is introduced by the 3° stepping interval of λ_0 along the ecliptic plane, but this smoothing is tolerated because of the relatively small sample size. Stars within 20° of the ecliptic plane ($|\beta| < 20^\circ$) were analyzed separately and are plotted as dashed lines in the top two panels. $C_{P\beta}$ represents the covariance between polarization P and ecliptic latitude β (eqn. 1 of Paper I). Fig. 1 also shows the direction of the large inflowing ISDGs observed by Ulysses and Galileo (§3) The polarization maximum seen near $\lambda_0 \sim 140^\circ$, with $\sim 1.8 \sigma$, is dominated by the three stars HD 98230, HD 78154 and HD 95128 at high ecliptic latitude. The conclusions of Paper I are reinforced by this extended data set.

3.1. Distance Dependence of Polarization

The mean polarization is independent of star distance for stars within ~ 30 pc, but increases by $\sim 1\sigma$ beyond 30 pc (Fig. 2). In contrast, the polarizations of the total sample of ~ 200 stars show no enhancement in the nearest 10 pc, and barely increase beyond 30 pc. There does not appear to be any significant change with distance in θ_C for the stars contributing to the P_{\max} region, however the statistics are poor since these are $\sim 2 - 3\sigma$ effects.

The nearest star showing polarization is 36 OphAB (HD 155886) at a distance of 5 pc, and located at $\ell = 358.3^\circ$, $b = +6.9^\circ$ ($\lambda = 260.0$, $\beta = -3.5^\circ$). This star is close to the ecliptic plane, 10° from the He $^\circ$ upwind direction, and with $P = 1.75 \pm 0.7 \times 10^{-4}$ and $\theta_C = -15^\circ$. Given the uncertainties and projection effects, this is consistent with $\langle \theta_C \rangle \sim -23^\circ$, averaged over the stars in the P_{\max} region (see the following section). A 1σ uncertainty in either Q or U translates to an uncertainty in the position angle of $\delta\theta_C = 3^\circ - 8^\circ$ for 36 OphAB. The relatively constant P value for the nearest 30 pc, of which 36 OphAB is an example, indicates the polarization is formed very close to the Sun.

3.2. Direction of Maximum Polarization

The polarization reaches a maximum, P_{\max} , at a position offset by $\Delta\lambda \sim +35^\circ$ from the heliosphere nose given by the large grains and He° (Fig. 1, top). The polarization maximum is strongest for stars close to the ecliptic plane, $|\beta| < 20^\circ$ (dashed line). Considering both P and θ_C in Fig. 1 indicates that the maximum polarization occurs at $\lambda=294^\circ \pm 7^\circ$ and $|\beta| < 20^\circ$ ($\ell \sim 19.2^\circ$, $b \sim -21.2^\circ$) with an uncertainty of $\sim 20^\circ$. Fig. 3 indicates the maximum is centered around $\lambda=294^\circ$, $\beta \sim -5^\circ$, or $\ell \sim 14.6^\circ$, $b \sim -23.8^\circ$. Presumably the polarization is no longer observable when the angle between the sightline and \hat{k}_B deviates significantly from 90° . This condition is easy to estimate, since the observed polarization is very weak and generally not much more than $\sim 3.0 \sigma$, while the minimum reliable polarization measurement is $\sim 2.5 \sigma$. Thus polarization will only be detectable in stars within $\sim 35^\circ$ of the perpendicular direction if the field lines are straight. The width of the band of observed polarization in Fig. 3 is $\sim 45^\circ$, which is not inconsistent with this estimate considering the uncertainties.

3.3. Polarization Position Angle

The consistency of θ_C in the P_{\max} region contributes to the reality of this weak polarization signal. The polarization position angle θ_C has a consistent value of $\theta_C \sim -23^\circ$ in the region of maximum polarization (Fig. 1, middle). Note that 36 OphAB is $\sim 35^\circ$ from the P_{\max} direction, but retains a consistent polarization angle. If the P_{\max} region corresponds to a sightline perpendicular to \vec{B}_{IS} , as expected, then $P_{\max} \sim 20 \times 10^{-5}$ projects to $P_{\max} \sim 17 \times 10^{-5}$ for the 36 OphAB direction, versus the observed value $\theta_C \sim -15^\circ$, which is within the uncertainties. Therefore, the position angles are consistent with P_{\max} corresponding to a sightline perpendicular to \vec{B}_{IS} . For the P_{\max} region centered at $\lambda \sim 294^\circ$, $\beta = -5^\circ$, and noting that the plane of polarization is approximately parallel to the galactic plane (T82), then \vec{B}_{IS} within 5 pc of the Sun is directed towards $\ell \sim 105^\circ$, $b \sim 0^\circ$, with an uncertainty of $\sim \pm 10^\circ$.

3.4. P - β Anticorrelation and Magnetic Wall

In the P_{\max} region, $\lambda=280^\circ$ – 330° , polarization strength anticorrelates with ecliptic latitude (Fig. 1, bottom). This conclusion is unchanged from Paper I, and is based on the full $\beta = \pm 50^\circ$ data set. The anticorrelation between P and β for $\beta < 0^\circ$ is the primary evidence that the polarization is created by aligned grains in the magnetic wall of the heliosphere. The magnetic wall is predicted to be at negative ecliptic latitudes during the 1970's for an

interstellar field directed towards $\sim 90^\circ$, when the solar wind and interstellar fields were parallel in the southern ecliptic hemisphere. The \vec{B}_{IS} field polarity is obtained from rotation measure data (e.g. Rand & Kulkarni 1989). Polarizations of stars within ~ 400 pc and pulsar rotation measure data yield similar orientations for the global nearby \vec{B}_{IS} , $\sim 83^\circ$ and $\sim 71^\circ$ respectively; the rotation measure data also give the field polarity, and global \vec{B}_{IS} near the Sun is directed towards $\ell \sim 71^\circ$ (Heiles 1996; Rand & Kulkarni 1989; Indrani & Deshpande 1999). A similar polarity is assumed for the LIC \vec{B}_{IS} , yielding parallel solar wind and interstellar magnetic fields in the southern ecliptic hemisphere, during the solar minima of the 1970's and 1990's, when the polarization and Ulysses data were acquired. For \hat{k}_{B} directed towards $\ell \sim 105^\circ$, during the 1970's the solar wind and interstellar field lines were antiparallel over the northern ecliptic hemisphere, so that reconnection would tangle the field lines and rapidly disrupt grain alignment.

The polarization data are plotted in ecliptic coordinates in Fig. 3, along with the positions of the galactic plane, 2.6 kHz emission events (KG03, §1), the upwind direction of the large inflowing dust grains (F99), and the upwind directions for H $^\circ$ and He $^\circ$ (W04, Lallement et al. 2005). Polarizations with $P > 2\sigma$ are plotted as filled symbols. The stars with the strongest polarization form a wide band ($> 45^\circ$) extending from the upwind to downwind direction. One side of the band extends through the points $(\lambda, \beta) \sim (270^\circ, -5^\circ)$, $(360^\circ, -15^\circ)$, to $(85^\circ, -40^\circ)$, and the second side dips to lower ecliptic latitudes and through $(\lambda, \beta) \sim (280^\circ, -45^\circ)$, $(360^\circ, -50^\circ)$, to $(40^\circ, -60^\circ)$. This band of weak polarization in the southern ecliptic hemisphere is offset towards the direction of solar rotation, when compared to a meridian passing through the upwind direction and south ecliptic pole.

4. Grain Alignment in Local Cloud

Most observed starlight polarization is formed in denser ISM, however the LIC grain composition appears similar to the olivines in the global ISM (§2.3) so that existing alignment theory can be applied. Magnetic alignment theories derive from the original discussion of Davis & Greenstein (1951, DG51),⁶ who proposed that magnetic torques align the principal inertial axis of the grain with the average angular momentum of asymmetric grains, \mathbf{J}_{avg} , and also align \mathbf{J}_{avg} with the magnetic field, \vec{B}_{IS} . Grain-gas collisions spin up grains so

⁶Davis is the same Leverett Davis, Jr., who originated the idea of the heliosphere by proposing that the momentum flux of solar corpuscular radiation formed a cavity of radius ~ 200 AU in the local galactic magnetic field (also see Parker 2001).

they acquire a random angular momentum with two parts, J_{avg} which precesses about \vec{B}_{IS} , and a stochastically varying angular momentum component related to the nutation of the asymmetric grain body inertial moment about J_{avg} . Torques both dissipate the component of J_{avg} perpendicular to \vec{B}_{IS} , and dampen grain nutation about J_{avg} . Uncertainties in the timescales for the magnetic alignment of grains relates primarily to these poorly understood, but heavily researched, torques (e.g., Davis & Greenstein 1951; Martin 1974; Purcell 1979; Lee & Draine 1985; Mathis 1986; Lee & Draine 1985; Roberge & Lazarian 1999; Lazarian 2000; Draine 2003; Lazarian 2003). If grain alignment in the global ISM is rapid and robust (Lazarian 2003), it will be even more robust in the LIC. I assume that ISDGs arrive at the heliosphere prealigned, so the outstanding question becomes whether these alignments can be randomized on relatively short time scales.

Lazarian (2003) discusses polarization by very small grains, $a \ll 0.06 \mu\text{m}$; such grains would be tightly coupled to \vec{B}_{IS} with gyroradii $< 10 \text{ AU}$ (F99). The LIC does not contain H_2 , so alternate processes would be required to generate any suprathermal rotation required to stabilize grain alignment against collisional disruption (Purcell 1979; Draine 1996). However, the disruption of grain alignment in the tenuous LIC occurs over timescales longer by factors of ~ 600 than in denser clouds (see below), so that suprathermal rotation is less important.

Grains are assumed to be silicates with density 3 gr cm^{-3} and a nearly spherical geometry. The LIC densities, temperature, and magnetic field strength are $n(\text{H}^0) \sim 0.2 \text{ cm}^{-3}$, $n(\text{e}) \sim 0.1 \text{ cm}^{-3}$, $n = n(\text{H}^0) + n(\text{e})$, $T_{\text{gas}} \sim 6300 \text{ K}$, and $|\vec{B}_{\text{IS}}| \sim 1.5 \mu\text{G}$ (§§2.1, 2.2). (also see Goodman & Whittet 1995). Mathis (1986) argues that grains with radii $a = 0.06 - 0.10 \mu\text{m}$ cause the polarization, based on the wavelength of maximum polarization, extinction and abundance constraints. The lower size limit originates with the requirement the grains are large enough to contain a superparamagnetic (SPM) inclusion (imaginary magnetic susceptibility $\mu'' > 0$). The SPM inclusion acts to increase the strength of the torque dissipating the grain body angular momentum, so that the average angular momentum vector J_{avg} and largest inertial axis co-align with each other and \vec{B}_{IS} (Davis & Greenstein 1951; Purcell 1979; Mathis 1986). Grains in this size range are excluded from the heliosphere for an initial $\vec{B}_{\text{IS}} > 1.5 \mu\text{G}$, and as field strengths rise as the grains approach the magnetic wall of the heliosphere.

4.1. Stability of Grain Alignment in Low Density ISM

There is a rich body of literature, stretching over 50 years, that associates interstellar polarization with asymmetric ISM opacities caused by magnetically aligned interstellar dust grains. However an important point to realize is that the LIC is warmer by a factor of

~ 100 , less dense by a factor of ~ 65 , and has plasma densities a factor of ~ 10 larger, than the typical clouds that have been discussed in the polarization literature. If the LIC and dense cloud magnetic field strengths are comparable to the ordered and random components of the global \vec{B}_{IS} ($\sim 1.6 \mu\text{G}$ and $\sim 5 \mu\text{G}$ respectively, Rand & Kulkarni 1989), then the magnetic field strength in the LIC is also a factor of ~ 4 weaker than the field strengths assumed in most polarization theory studies. Collisions between gas and grains provide the primary means of disrupting grain alignment. In the LIC, with density $n \sim 0.3 \text{ cm}^{-3}$ and temperature $T \sim 6300 \text{ K}$, the rate of these collisions is down by a factor of $\sim n/\sqrt{T} \sim 600$ compared to denser clouds. *Therefore, even though \vec{B}_{IS} is weaker, it is fundamentally easier to magnetically align ISDGs in the LIC than in denser clouds.* The following discussion assumes that grains are magnetically aligned in the upwind gas, and arrive prealigned to the heliosphere vicinity with perhaps some alignment enhancement as \vec{B}_{IS} is compressed at the heliosphere.

Several arguments indicate that stochastic processes do not affect grain alignment in the heliosphere-ISM interaction region. Grain alignment in the LIC will be disrupted at least as often as grains accumulate their own mass in thermal collisions with the gas, which occurs over timescales of $\tau_{\text{mass}} \sim 10^6 a \rho_{\text{gr}} / n \sqrt{T_{\text{gas}}}$ Myrs = 0.7–1.2 Myrs. The rotational damping time is $\tau_{\text{d}} \sim 0.6 \tau_{\text{mass}}$ for symmetric grains (in this case cubical, Lazarian & Draine 1997). These timescales are long compared to the ~ 30 years required for a dust grain to cross the bow shock and approach the heliopause.

In contrast, torques that dampen grain body nutation about J_{avg} occur over short timescales. Elastic collisions between thermal gas particles and spherical grains with $a \sim 0.1 \mu\text{m}$ radius will spin the grains about the grain-body principal axis at a mean angular velocity of $\omega \sim 3 \times 10^4 \sqrt{T_{\text{gas}}} / \sqrt{a_{\mu}^5 \rho} \sim 1.3 \times 10^6 \text{ s}^{-1}$. This “thermal” rotation induces a magnetic susceptibility of $K(\omega) = \mu'' / \omega \sim 10^{-13} \text{ s}$, which can be enhanced to $\sim 2 \times 10^{-8} \text{ s}$ if 1% of the grain material is contained in SPM clusters with ~ 5000 Fe atoms (Draine 1996), and which shortens the magnetic damping time to ~ 5 years (Roberge & Lazarian 1999). The magnetic moment induced by the rotating grain charge is also enhanced by the Barnett effect, where grain body angular momentum is dissipated by interactions with the grain lattice, and which dampens grain nutation and increases magnetic alignment efficiency. (Lazarian 2003; Roberge & Lazarian 1999). Therefore, apparently stochastic mechanisms do not disrupt the alignment of LIC ISDGs arriving at the heliosphere, and for the most optimal assumptions alignment may increase on time scales of ~ 5 years when interstellar field lines are compressed at the heliosphere.

4.2. Grain Charge and Gyroradius

The outer heliosheath regions filter out small charged grains. As ISDGs approach the heliosphere, grains with small charge-to-mass ratios, Q/m_{gr} follow the neutral gas into the heliosphere. Grains with large Q/m_{gr} ratios, together with interstellar plasma components, are trapped by \vec{B}_{IS} as field lines drape over the heliosphere (F99, Kimura & Mann 1998). During this interaction, grain gyroradii, l_{gyro} , vary with \vec{B}_{IS} and grain charging rates. For grain velocity V_{gr} , $l_{\text{gyro}} = m_{\text{gr}} V_{\text{gr}} / eZ |\vec{B}_{\text{IS}}|$, where $Z = 4\pi\epsilon_o a U_{\text{ES}}$ is a function of the electrostatic grain potential U_{ES} , and $\epsilon_o = 8.9 \times 10^{-14} \text{ C V}^{-1} \text{ cm}^{-1}$ is the permittivity (F99). U_{ES} is determined partially by photoelectric emission rates and collisional grain charging. In the LIC, $U_{\text{ES}} \sim 0.7 - 1.4 \text{ V}$ for $a = 0.06 - 0.1 \mu\text{m}$ (e.g. Weingartner & Draine 2001). For $V_{\text{gr}} = 26 \text{ km s}^{-1}$, $a \sim 0.1 \mu\text{m}$, and $|\vec{B}_{\text{IS}}| = 1.5 \mu\text{G}$, $l_{\text{gyro}} \sim 130 - 175 \text{ AU}$; for $a \sim 0.06 \mu\text{m}$, $l_{\text{gyro}} \sim 35 - 50 \text{ AU}$. The factor of ~ 2 jump in $|\vec{B}_{\text{IS}}|$ at the bow shock, and again near the heliopause, decreases l_{gyro} (Linde 1998). The self-consistent treatment in F99 of grain charging and \vec{B}_{IS} compression at the heliosphere indicates that for $|\vec{B}_{\text{IS}}| = 1.5 \mu\text{G}$ and radiation field parameter $G_o \sim 0$, grains with $a \lesssim 0.06 \mu\text{m}$ are excluded at the bow shock, and grains with $a \lesssim 0.15 \mu\text{m}$ are excluded at the heliopause. Grains with radii $a < 0.01 \mu\text{m}$ are excluded from the heliosphere under nearly all conditions. Analogous results were found by Kimura & Mann (1998) for strong fields, $\vec{B}_{\text{IS}} \sim 13 \mu\text{G}$, such that trajectories of grains with $a < 2 \mu\text{m}$ were found to be altered upwind of the heliopause. Grains in the size range of the Mathis polarizing grains, $0.06 - 0.1 \mu\text{m}$, are excluded from the heliosphere.

4.3. Slowly Changing \vec{B}_{IS}

In general, for magnetically aligned ISDGs the polarization maximum is observed where the sightline is perpendicular to the field direction. However, as the LIC interacts with the region beyond the heliopause, either grain alignment does or does not follow the slowly changing direction of \hat{k}_{B} . Lazarian (2003) argues that the fast Larmor precession, τ_{Lar} , induced by the Barnett effect proceeds at a period of $\tau_{\text{Lar}} \sim 15/B_{\text{IS}} \text{ s} \sim 0.3 \text{ years}$ for $|\vec{B}_{\text{IS}}| = 1.5 \mu\text{G}$. If this short timescale truly characterizes the alignment adjustment of grains in a slowly varying \hat{k}_{B} , then the maximum polarization direction will trace the perpendicular of the local field direction, rather than the “fossil” perpendicular direction indicated by grains that do not realign quickly enough beyond the heliopause. The transfer properties of the Stokes parameter Q over distances that are small compared to variations in \hat{k}_{B} indicates that weak polarization is weakly enhanced, and this case should apply near the heliosheath (Nee &

Jokipii 1979).

5. Discussion and Conclusions

The composition of LIC dust can be found from radiative transfer models, and the assumption that a solar abundance’s worth of atoms are either in the dust or the gas. The resulting LIC dust composition indicates olivines, that are perhaps similar to the amorphous olivines that dominate the SgrA* sightline (§2.3). Significant quantities of carbonaceous grains can be ruled out. These grains give a gas-to-dust mass ratio of $R_{g/d} \sim 200$, which is greater than the *in situ* value of $R_{g/d} < 130$ (§2.4). This indicates that the gas and dust may have decoupled over the LIC cloud lifetime, which in turn negates the underlying assumption that the reference abundance for an interstellar cloud is constant over small spatial scales. This contradiction may arise from the poorly understood reference abundance for the ISM.

The small interstellar grains causing the polarization, with high Q/M , trace \vec{B}_{IS} at the heliosphere, while large grains with low Q/M couple to the LIC velocity. The gyroradii of grains interacting with the heliosphere in the presence of a weak \vec{B}_{IS} has been studied previously, and grains with radii 0.06–0.10 μm are excluded, $l_{\text{gyro}} < 50$ AU, as the interstellar field compresses against the heliosphere.

An offset of $\Delta\lambda \sim +35^\circ$ between the direction of maximum polarization P_{max} and the upwind direction, found in Paper I, is confirmed with the addition of the Pirola data (§3). Evidently this offset does not act like a dumb compass needle, since grain alignment traces the coupling between the grain angular momentum and \vec{B}_{IS} .

A band of weak polarization, $\sim 2\sigma - 3\sigma$, stretches through the southern ecliptic hemisphere between the P_{max} region and the downwind direction. The width of the band in the upwind direction is consistent with the detectability limits of the polarization (§3.2). The band shows an offset towards the direction of positive solar rotation when compared to a meridian between the upwind direction and south ecliptic pole.

Consistent position angles for polarizations in the upwind direction, and the relative constancy of polarization with star distance, indicate that that polarization is formed within 5 pc of the Sun. Polarization data are also consistent with P_{max} occurring in a sightline perpendicular to the interstellar magnetic field direction, \hat{k}_B , because the polarization towards 36 OphAB is decreased by the cosine of the angle between the star and P_{max} direction.

The position angles of the polarization in the P_{max} region are relatively parallel to the galactic plane (§3.3). Together with the P_{max} direction of $\ell \sim 15^\circ$, it then appears that \vec{B}_{IS}

is oriented towards $\ell \sim 105^\circ$, $b \sim 0^\circ$ with $\sim \pm 10^\circ$ uncertainties. This conclusion makes use of grain alignment theories that indicate the plane of polarization is parallel to \vec{B}_{IS} . If the polarity of the LIC \vec{B}_{IS} is similar to the polarity of the global field found from rotation measure data, then the field is directed towards $\ell \sim 105^\circ$. In this case, the interstellar and solar wind magnetic fields were parallel in the southern ecliptic hemisphere during the solar minimum of the 1970's when the polarization data were acquired, and again during the 1990's minimum when much of the Ulysses dust data were obtained. This \hat{k}_{B} direction gives an angle between the inflowing neutral gas and \vec{B}_{IS} of $\sim 75^\circ$.

In low density ISM such as the LIC, the disruption of grain alignment is ~ 600 times slower than in the denser clouds for which grain alignment theory has been developed (§4.1). It takes on the order of 10^6 years for grain alignment to disrupt by sweeping up its own mass in collisions. The ISDGs are assumed to arrive prealigned at the heliosphere, and collisional disruption of alignment in the LIC is too slow to be meaningful.

Despite the fact that grain alignment theories are still somewhat uncertain, collisions between gas particles and grains occur rapidly enough to allow magnetic torques to quickly dissipate the nutation of the grain body moment of inertia about the average angular momentum, J_{avg} , so that grain alignment is quick and robust even in low density ISM. Estimates place the alignment on the order of years because of the Barnett effect (§4), so the alignment of grains near the heliosphere will respond rapidly to the slowly varying direction of \vec{B}_{IS} . If \vec{B}_{IS} becomes tangled or reconnects with the solar wind magnetic field, as happened in much of the northern ecliptic hemisphere during the 1970's solar minimum according to this P_{max} direction, then the polarization should vanish. The compression of the interstellar magnetic field in the outer heliosheath regions, by a factor of ~ 5 , boosts grain alignment. During solar minimum conditions the solar magnetic field is dominated by open field lines with a dipole component, in contrast to solar maximum conditions when the quadrupole and hexapole moments dominate, making the solar wind magnetic field in the outer heliosphere more disorderly (Bravo et al. 1998).

Polarization will vanish where the field direction changes rapidly, is turbulent over smaller scales than the grain gyroradius, or where the interstellar and solar wind magnetic field are anti-parallel.

The offset of P_{max} corresponds to the secondary peak in energetic neutral atom (ENA) fluxes found by Collier et al. (2004). ENAs originate in charge exchange between the plasma component and interstellar H^0 , which will happen inside of the orderly field region that is required by the aligned grains. However, since an orderly \vec{B}_{IS} will pinch off the plasma as it compresses against the heliospheric magnetic field, it is understandable that the P_{max}

and ENA positions overlap (see Fig. 2). Collier, however (private communication), has suggested that ENA's may form by charge exchange between H^0 and the grains. Since most of the surface area of the ISDGs are in the small grain component that is excluded from the heliosphere, this also is not unreasonable.

Finally, based on this analysis, there are two broad possibilities that emerge. It appears that sensitive observations of the polarization of nearby stars over long time scales will provide a ground-based monitor of the region where the heliosphere interacts with the ISM. The second possibility is that interstellar dust interacting with the heliosphere provides a low- l contaminant of the cosmic microwave background emission and/or polarization data. For this second case, the symmetries of the dust-heliosphere interaction are strongly broken by the solar cycle, for both large and small grains (but for different reasons). These broken symmetries should be evident from comparisons between solar minimum and solar maximum data, and between data acquired over different solar magnetic polarities.

This research has been supported by the NASA the grants NAG5-13107 and NNG05GD36G to the University of Chicago.

REFERENCES

- Altobelli, N., Krüger, H., Moissl, R., Landgraf, M., & Grün, E. 2004, *Planet. Space Sci.*, 52, 1287
- Asplund, M., Grevesse, N., & Sauval, A. J. 2005, in *ASP Conf. Ser. 336: Cosmic Abundances as Records of Stellar Evolution and Nucleosynthesis*, 25–+
- Baguhl, M., Gruen, E., & Landgraf, M. 1996, *Space Science Reviews*, 78, 165
- Bochkarev, N. G. 1987, *Ap&SS*, 138, 229
- Bravo, S., Stewart, G. A., & Blanco-Cano, X. 1998, *Sol. Phys.*, 179, 223
- Breitschwerdt, D., Freyberg, M. J., & Egger, R. 2000, *A&A*, 361, 303
- Burlaga, L. F., Ness, N. F., Acuña, M. H., Lepping, R. P., Connerney, J. E. P., Stone, E. C., & McDonald, F. B. 2005, *Science*, 309, 2027
- Cairns, I. H. 2004, in *AIP Conf. Proc. 719: Physics of the Outer Heliosphere*, 381–386
- Chiar, J. E. & Tielens, A. G. G. M. 2006, *ApJ*, 637, 774

- Collier, M. R., Moore, T. E., Simpson, D., Roberts, A., Szabo, A., Fuselier, S. A., Wurz, P., Lee, M. A., & Tsurutani, B. T. 2004, *Adv. Space Res.*, 34, 166
- Davis, L. J. & Greenstein, J. L. 1951, *ApJ*, 114, 206
- Decker, R. B., Krimigis, S. M., Roelof, E. C., Hill, M. E., Armstrong, T. P., Gloeckler, G., Hamilton, D. C., & Lanzerotti, L. J. 2005, *Science*, 309, 2020
- Dorschner, J. & Henning, T. 1995, *A&A Rev.*, 6, 271
- Draine, B. T. 1996, in *ASP Conf. Ser. 97: Polarimetry of the Interstellar Medium*, ed. W. G. Roberge & D. C. B. Whittet, 16–+
- Draine, B. T. 2003, *ARA&A*, 41, 241
- Frisch, P. C. 1981, *Nature*, 293, 377
- Frisch, P. C. 1990, in *Physics of the Outer Heliosphere*, ed. S. Grzedzielski & D. E. Page, 19–22
- . 1995, *Space Sci. Rev.*, 72, 499
- . 1996, *Space Sci. Rev.*, 78, 213
- . 2005, *ApJ*, 632, L143
- Frisch, P. C., Dorschner, J. M., Geiss, J., Greenberg, J. M., Grün, E., Landgraf, M., Hoppe, P., Jones, A. P., Krätschmer, W., Linde, T. J., Morfill, G. E., Reach, W., Slavin, J. D., Svestka, J., Witt, A. N., & Zank, G. P. 1999, *ApJ*, 525, 492
- Frisch, P. C., Grodnicki, L., & Welty, D. E. 2002, *ApJ*, 574, 834
- Frisch, P. C., Müller, H. R., Zank, G. P., & Lopate, C. 2005, in *Astrophysics of Life*, 21–34
- Frisch, P. C. & Slavin, J. D. 2003, *ApJ*, 594, 844
- Frisch, P. C. & Slavin, J. D. 2005, *Advances in Space Research*, 35, 2048
- Frisch, P. C. & York, D. G. 1983, *ApJ*, 271, L59
- Goodman, A. A. & Whittet, D. C. B. 1995, *ApJ*, 455, L181+
- Grevesse, N. & Sauval, A. J. 1998, *Space Science Reviews*, 85, 161
- Grün, E., Srama, R., Krüger, H., Kempf, S., Dikarev, V., Helfert, S., & Moragas-Klostermeyer, G. 2005, *Icarus*, 174, 1

- Grun, E., Zook, H. A., Baguhl, M., Balogh, A., Bame, S. J., Fechtig, H., Forsyth, R., Hanner, M. S., Horanyi, M., Kissel, J., Lindblad, B.-A., Linkert, D., Linkert, G., Mann, I., McDonnell, J. A. M., Morfill, G. E., Phillips, J. L., Polanskey, C., Schwehm, G., Siddique, N., Staubach, P., Svestka, J., & Taylor, A. 1993, *Nature*, 362, 428
- Gry, C. & Jenkins, E. B. 2001, *A&A*, 367, 617
- Heiles, C. 1996, *ApJ*, 462, 316
- Heiles, C. & Troland, T. H. 2003, *ApJS*, 145, 329
- Holweger, H. 2001, in *AIP Conf. Proc. 598: Joint SOHO/ACE workshop "Solar and Galactic Composition"*, 23–+
- Indrani, C. & Deshpande, A. A. 1999, *New Astronomy*, 33
- Jones, A. P., Tielens, A., & Hollenbach, D. J. 1996, *ApJ*, 469, 740
- Kemper, F., Vriend, W. J., & Tielens, A. G. G. M. 2004, *ApJ*, 609, 826
- Kimura, H. & Mann, I. 1998, *ApJ*, 499, 454
- Kurth, W. S. & Gurnett, D. A. 2003, *J. Geophys. Res.*, 108, 2
- Lagache, G., Haffner, L. M., Reynolds, R. J., & Tufte, S. L. 2000, *A&A*, 354, 247
- Lallement, R., Quémerais, E., Bertaux, J. L., Ferron, S., Koutroumpa, D., & Pellinen, R. 2005, *Science*, 307, 1447
- Landgraf, M. 2000, *J. Geophys. Res.*, 105, 10303
- Landgraf, M., Baggaley, W. J., Grün, E., Krüger, H., & Linkert, G. 2000, *J. Geophys. Res.*, 105, 10343
- Lazarian, A. 2000, in *ASP Conf. Ser. 215*, 69
- Lazarian, A. 2003, *Journal of Quantitative Spectroscopy and Radiative Transfer*, 79, 881
- Lazarian, A. & Draine, B. T. 1997, *ApJ*, 487, 248
- Lee, H. M. & Draine, B. T. 1985, *ApJ*, 290, 211
- Linde, T. J. 1998, PhD thesis, Univ. of Michigan, Ann Arbor, <http://hpcc.engin.umich.edu/CFD/publications>

- Lodders, K. 2003, *ApJ*, 591, 1220
- Möbius, E., Bzowski, M., Chalov, S., Fahr, H.-J., Gloeckler, G., Izmodenov, V., Kallenbach, R., Lallement, R., McMullin, D., Noda, H., Oka, M., Pauluhn, A., Raymond, J., Ruciński, D., Skoug, R., Terasawa, T., Thompson, W., Vallergera, J., von Steiger, R., & Witte, M. 2004, *A&A*, 426, 897
- Martin, P. G. 1974, *ApJ*, 187, 461
- Mathis, J. S. 1986, *ApJ*, 308, 281
- Nee, S. F. & Jokipii, J. R. 1979, *ApJ*, 234, 140
- Parker, E. N. 2001, *A History of the Solar Wind Concept* ("Kluwer Academic Publishers"), 225–255
- Pirola, V. 1977, *A&AS*, 30, 213
- Pogorelov, N. V., Zank, G. P., & Ogino, T. 2004, *ApJ*, 614, 1007
- Purcell, E. M. 1979, *ApJ*, 231, 404
- Rand, R. J. & Kulkarni, S. R. 1989, *ApJ*, 343, 760
- Roberge, W. G. & Lazarian, A. 1999, *MNRAS*, 305, 615
- Routly, P. & Spitzer, L., J. 1952, *ApJ*, 115, 227
- Slavin, J. D. & Frisch, P. C. 2002, *ApJ*, 565, 364
- . 2006a, in preparation
- . 2006b, *ApJ*, in preparation
- Slavin, J. D., Jones, A. P., & Tielens, A. G. G. M. 2004, *ApJ*, 614, 796
- Stone, E. C., Cummings, A. C., McDonald, F. B., Heikkila, B. C., Lal, N., & Webber, W. R. 2005, *Science*, 309, 2017
- Tinbergen, J. 1982, *A&A*, 105, 53
- Weingartner, J. C. & Draine, B. T. 2001, *ApJS*, 134, 263
- Whittet, D. C. B. 2004, in *ASP Conf. Ser. 309: Astrophysics of Dust*, ed. A. N. Witt, G. C. Clayton, & B. T. Draine, 65–+

Witte, M. 2004, *A&A*, 426, 835

Zank, G. P. 1999, *Space Science Reviews*, 89, 413

Zubko, V., Dwek, E., & Arendt, R. G. 2004, *ApJS*, 152, 211

Table 1. Composition of Interstellar Dust in the Cloud feeding Gas and Dust into the Heliosphere

Element	LIC ^a Gas PPM	Solar ^b Composition PPM	LIC ^c Dust PPM
C	263–275	288	13–25
N	50.1 – 52.5	79	26.5 – 28.9
O	380	575	195
Mg	4.68 – 4.90	41.7	36.8 – 37.0
Al	0.0794	3.47	3.39
Si	6.03	40.7	34.7
Fe	1.86	34.7	32.8

^aThe LIC gas-phase densities are from radiative transfer Models 2 and 8 in Slavin & Frisch (2002), also see Frisch & Slavin (2003).

^bThe solar composition is from Lodders (2003).

^cThe dust composition is given by the solar minus gas composition.

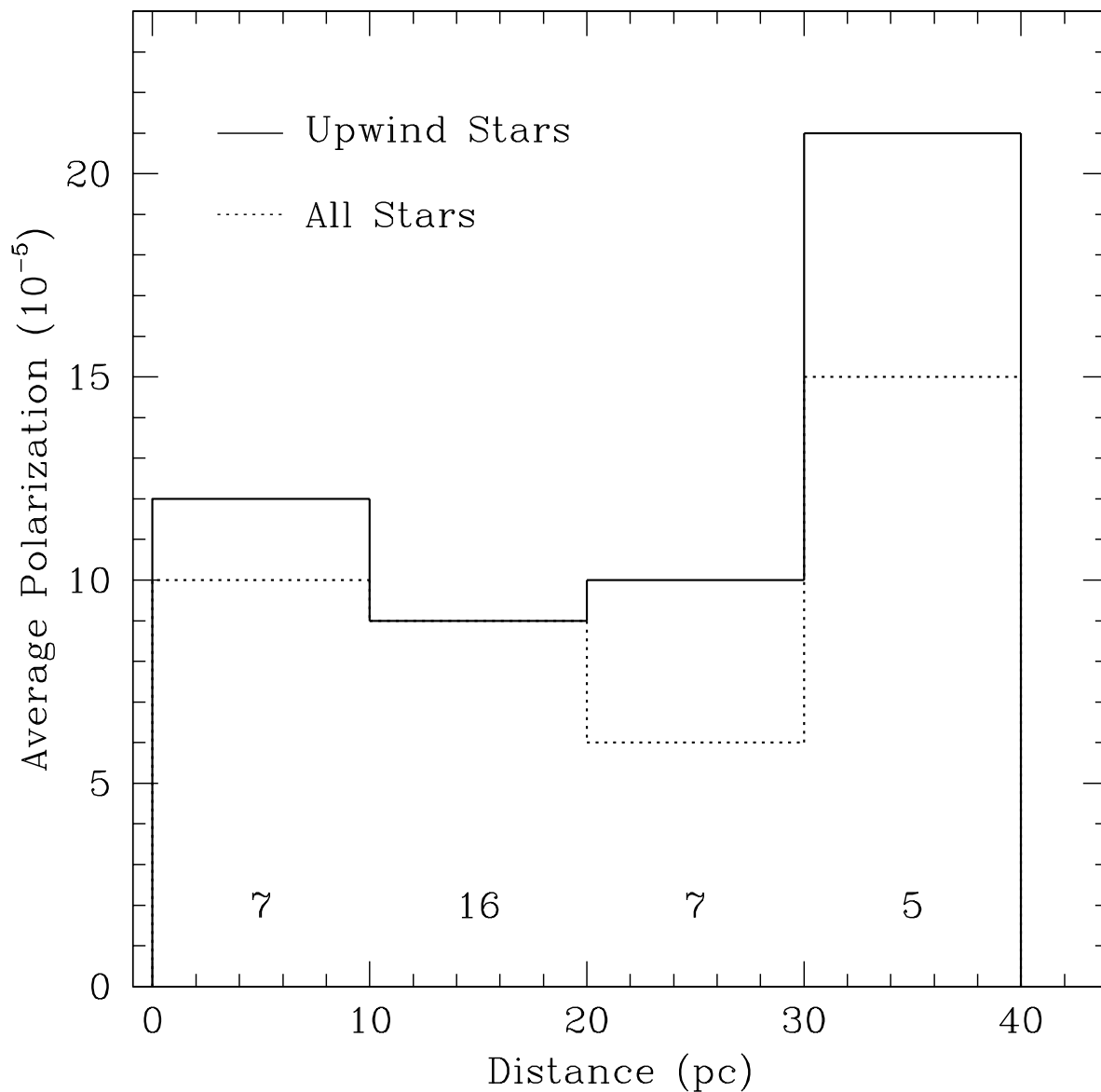


Fig. 1.— Histogram of the average polarization for stars binned into distance intervals of 10 pc. The polarization units are 10^{-5} degree of polarization, and 1σ uncertainties are $\sim 7 \times 10^{-5}$. The solid line includes only stars towards the heliosphere nose ($330^\circ < \ell < 40^\circ$ and $|b| < 50^\circ$), with the numbers of stars in each bin shown at the bottom. The dotted line includes all stars within 40 pc.

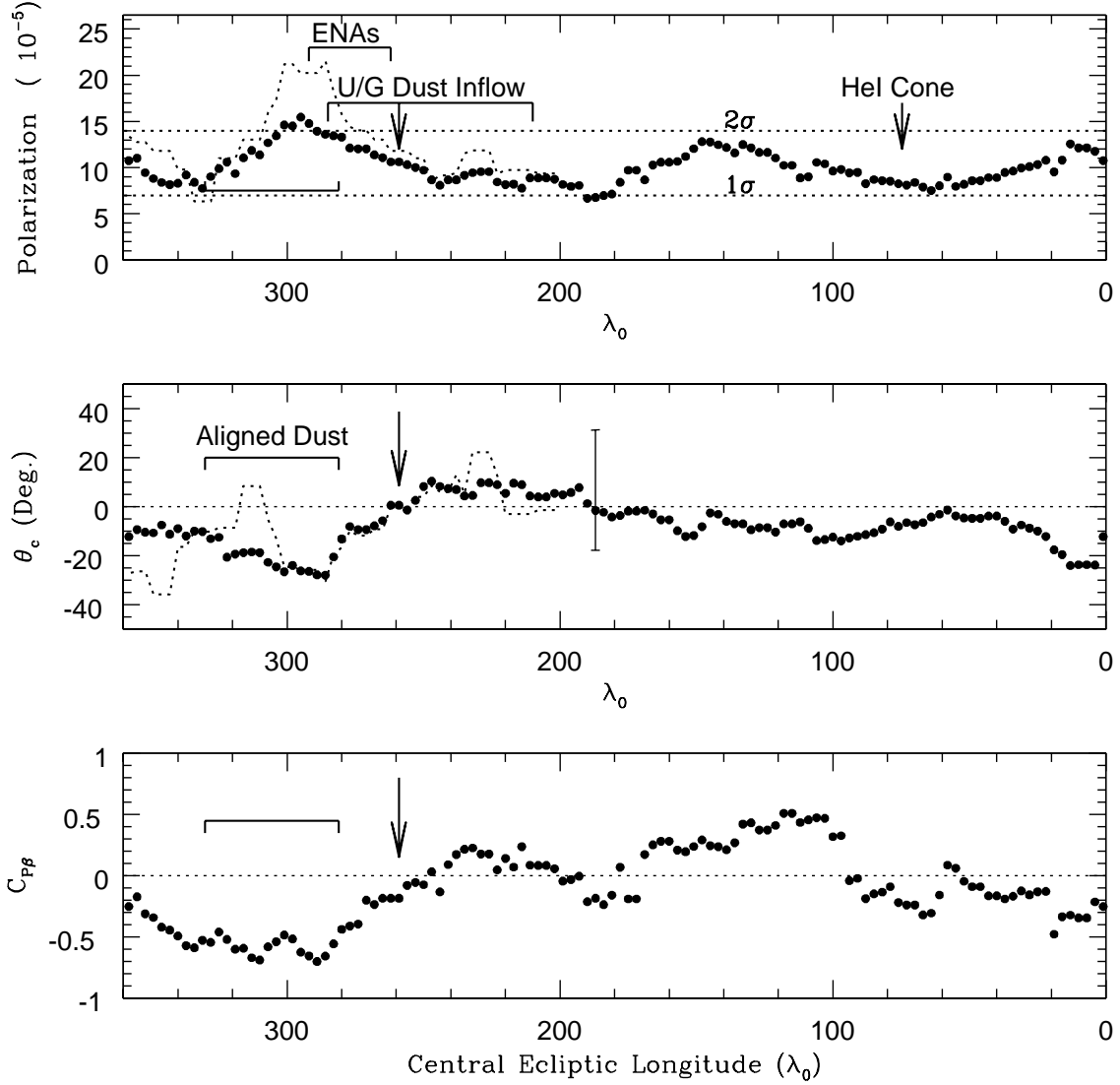


Fig. 2.— Polarization Properties as a Function of Ecliptic Latitude: Top: The average polarization P for stars with $|\beta| < 50^\circ$ is plotted as dots, and for stars with $|\beta| < 20^\circ$ as a dashed line. Data are averaged over $\pm 20^\circ$ in ecliptic longitude, λ . The direction of maximum P is shifted by $\sim 20\text{--}30^\circ$ from the upwind direction of the large interstellar dust grains detected by Ulysses/Galileo (Frisch et al. 1999), and upwind gas and dust directions differ by $\sim 5^\circ$. Middle: The averaged polarization position angle *in celestial coordinates*, θ_C . In the region of maximum polarization, $\lambda \sim 280^\circ \rightarrow 310^\circ$, the grains show consistent position angles. Bottom: The correlation coefficient between P (top) and β is shown as a function of the ecliptic longitude. The strongest polarization is found at negative ecliptic latitudes.

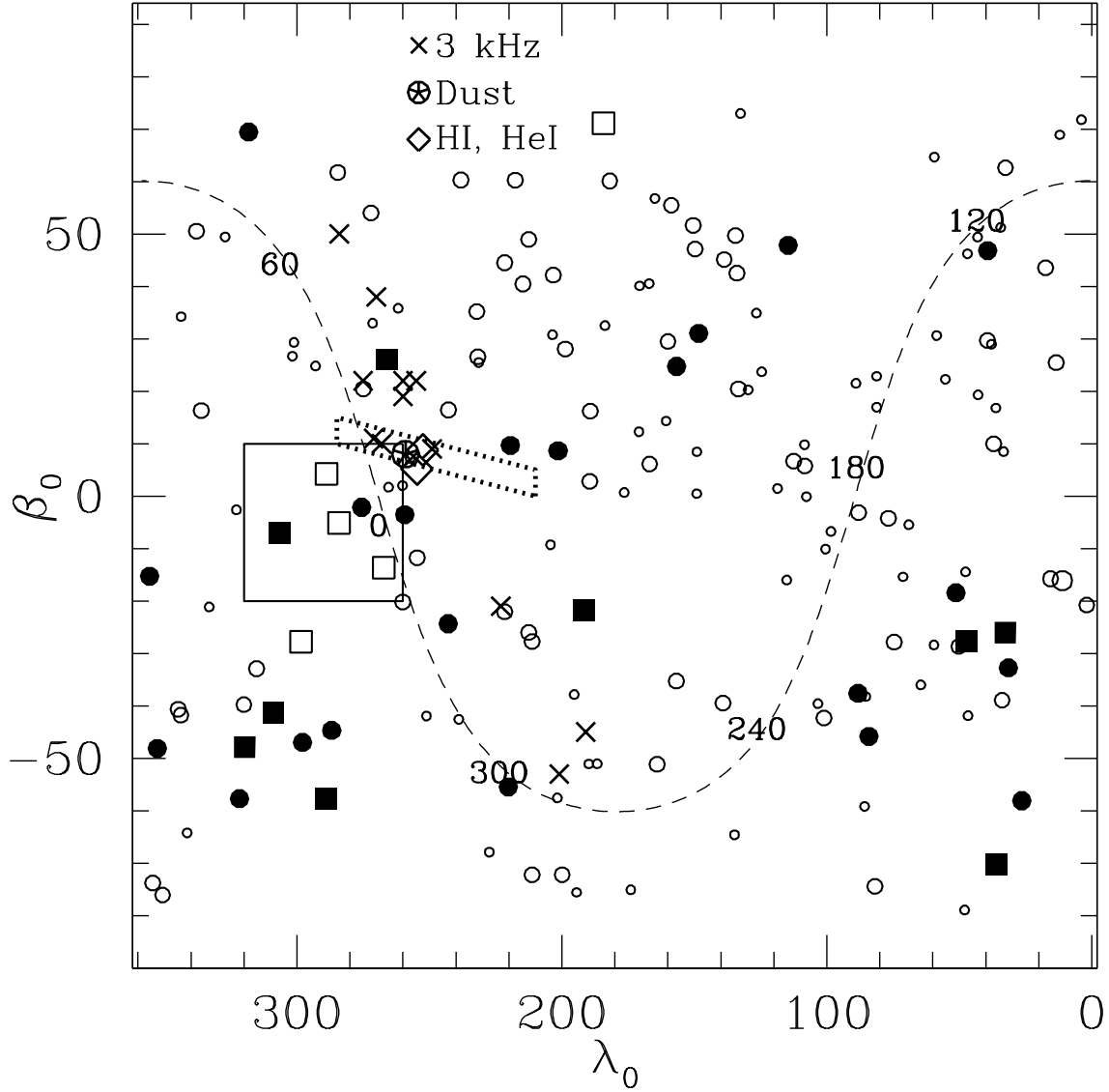


Fig. 3.— The distribution of polarization is shown in ecliptic coordinates. A region of polarization with similar position angles is seen towards the heliosphere nose (solid line box, see Fig. 2 or Fig. 6 of T82). A band of polarization extends at negative β 's from the heliosphere nose towards the downwind direction, which is at $\lambda \sim 75^\circ$, $\beta \sim -5^\circ$. The upwind direction of inflowing dust grains, H° , and He° are indicated by the circled star and open diamonds. The 3 kHz emission event locations are plotted as “X’s”. The dotted-line box shows the uncertainties on the upwind dust direction (Frisch et al. 1999). The solid-line box shows the region of maximum P from Figure 2. The galactic plane is shown as the dashed line labeled by galactic longitude. The boxes and circles represent stars with polarization $P > 3\sigma$ and $P = 2\sigma - 3\sigma$, respectively. The filled symbols represent stars within 30 pc, and the open symbols show stars with distances 30–40 pc. The large and small open circles indicate, respectively, $P = 1\sigma - 2\sigma$ and $P < 1\sigma$.